

In situ determination of the quantum yield of phytoplankton chlorophyll *a* fluorescence: A simple algorithm, observations, and a model

J. Ruairidh Morrison

Woods Hole Oceanographic Institution, Woods Hole, Massachusetts 02543

Abstract

Vertical profiles of the in situ quantum yield of fluorescence of chlorophyll *a*, ϕ_f , were derived with an algorithm from spectral underwater radiometer measurements. Select inherent optical properties were obtained from an initial radiance reflectance inversion that was optimized by comparing retrieved estimates of phytoplankton absorption with independent measurements. The comparison of chlorophyll concentrations produced by the algorithm to measured values allowed validation of the inversion. Fluorescence quantum yield values were calculated from the retrieved phytoplankton absorption and the upwelling radiance corrected for elastic and inelastic scattering. Raman scattered light was found to be a significant component of the upwelling light field at wavelengths of Chl *a* fluorescence. Values of ϕ_f determined using the algorithm, and therefore derived solely from the radiometer measurements, were not significantly different from those estimated using independent measurements of absorption by phytoplankton ($r^2 = 0.86$). The profiles of ϕ_f were characterized by an initial increase with depth to a subsurface maximum followed by a subsequent decrease. The irradiances of the subsurface maxima and ϕ_f at high irradiances appeared to be well conserved. An irradiance-based model including photochemical and nonphotochemical quenching was developed to explain variations in the quantum yield.

Variations in phytoplankton biomass have been studied using sun stimulated fluorescence, often termed natural or passive fluorescence, which can be detected as red peaks in both in-water (Gordon 1979; Kishino et al. 1984; Topliss 1985; Kiefer et al. 1989; Fischer and Kronfeld 1990; Stegmann et al. 1992; Roesler and Perry 1995; Babin et al. 1996; Culver and Perry 1997; Hu and Voss 1998; Maritorea et al. 2000) and water-leaving radiance spectra (Neville and Gower 1977; Gower 1980; Doerffer 1981). Global scale measurements are possible using satellite sensors capable of resolving these fluorescence peaks (e.g., Esaias et al. 1998; Gower et al. 1999) and may be of particular advantage in case II waters, where suspended particulate matter and colored dissolved organic matter (CDOM) can interfere with chlorophyll algorithms based on blue-green ratios (Gower et al. 1999). The derivation of primary production from sun-stimulated fluorescence has also been proposed (e.g., Topliss and Platt 1986; Kiefer et al. 1989; Chamberlin et al. 1990; Chamberlin and Marra 1992; Kiefer and Reynolds 1992; Stegmann et al. 1992) and will be incorporated into satellite sensor mission data products (Esaias et al. 1998).

Scattering of light, both elastic and inelastic, is responsible for redirecting incident photons into the upwelling light stream (Mobley 1994). Elastic scattering reflects ambient solar radiation, whereas inelastic scattering involves a shift in wavelength and includes chlorophyll fluorescence. At environmental temperatures, the majority of chlorophyll *a* fluo-

rescence comes from photosystem II (PSII), the contribution from photosystem I being negligible (Falkowski and Kiefer 1985; Kiefer and Reynolds 1992). Both in situ and cultured fluorescence emissions have been characterized using a Gaussian peak centered around 683 nm with a 10.6-nm standard deviation (Gordon 1979; Prézelin and Ley 1980; Kishino et al. 1984; Collins et al. 1985), and the emission appears to be spectrally independent of the excitation wavelength (Myers and Graham 1963). Raman scattering by water, with excitation wavelengths around 555 nm, is another potential inelastic source (Berwald et al. 1998; Maritorea et al. 2000). The high absorption of water at red wavelengths compared with those in the blue and green regions of the spectrum leads to increasing dominance of inelastically scattered light at chlorophyll fluorescence wavelengths with increasing depth (Kishino et al. 1984; Kiefer et al. 1989). This also means that >90% of the upwelled red quanta originate from within 5 m below, even in the clearest oceans (Topliss 1985), which limits the resolution of satellite-based measurements to a thin layer at the top of the water column (Babin et al. 1996).

Instruments to measure the upwelling light field and resolve the chlorophyll fluorescence signal have varied from single-waveband radiance sensors targeting the emission peak (Kiefer et al. 1989; Chamberlin et al. 1990) to spectrally resolved irradiance meters (Kishino et al. 1984; Roesler and Perry 1995; Culver and Perry 1997; Maritorea et al. 2000). A variety of techniques have been used to partition the upwelling light into fluoresced and nonfluoresced contributions. Spectral measurements allowed linear interpolation between upwelling radiation at two wavelengths on either side of the fluorescence peak to define background and fluorescence signals (Gordon 1979; Kishino et al. 1984; Doerffer 1993; Culver and Perry 1997; Maritorea et al. 2000). It has commonly been assumed that only chlorophyll fluorescence and elastically scattered light are important sources of upwelled red light (Chamberlin et al. 1990; Roes-

Acknowledgments

The work was funded by a U.K. N.E.R.C. studentship (GT4/93/260/P) and was enabled by U.K. M.A.F.F. grant CAS 2844, U.K. N.E.R.C. grant GST/02/970, and the U.K. N.E.R.C. LOIS Shelf Edge Study Community Program. Additional support was provided by the NASA SIMBIOS contract (NAS5-00198). I thank Heidi Sosik, Norm Nelson, Dave Bowers, Paul Tett, and Dave Mills for their support and advice, as well as the ship crew and personnel involved in the data collection. WHOI contribution 10610.

ler and Perry 1995). The presence of the background, or baseline, signal at depths where elastically scattered light should have been negligible (Culver and Perry 1997) has been attributed to Raman scattering and can constitute 20% of the upwelled light (Maritorena et al. 2000). Not accounting for Raman scattering in partitioning will lead to an overestimation of the fluorescence signal.

Incident irradiance, phytoplankton absorption, and the quantum yield of fluorescence (ϕ_f) are the primary factors controlling fluorescence output (Falkowski and Kiefer 1985; Kiefer et al. 1989). Sources of variability in the absorption spectrum include both phylogenetic and physiological—inter- and intra-species differences in pigment composition, cellular organization, and the package effect (Morel and Bricaud 1981; Bidigare et al. 1987; Sosik et al. 1989; Falkowski and Laroche 1991; Babin et al. 1993). The quantum yield of fluorescence is simply the ratio of the photons emitted to those absorbed. Its regulation, or quenching, can be divided into two distinct regimes: (1) photochemical quenching, where there is a direct trade-off with the quantum yield of photosynthesis and thus a theoretical basis for the prediction of primary production from fluorescence, and (2) nonphotochemical quenching related to various stresses, where the relationship between the fluorescence and photosynthetic quantum yields is uncertain (Kiefer and Reynolds 1992).

Photochemical quenching, q_p , may be considered in terms of the state of the PSII reaction centers. A reaction center may be considered open, or unexcited, when available to do photochemical work and closed, or excited, when in the process of doing work. The number of open and closed reaction centers changes rapidly, on a timescale of microseconds, with changes in the intensity of the exciting radiation. As the proportion of open reaction centers increases, the quantum efficiency of fluorescence decreases and the quantum efficiency of photochemistry increases in a complimentary linear fashion. Kiefer and Reynolds (1992) modeled ϕ_f on the basis of the single step probabilities of state transitions within the reaction center. This can be simplified to describe photochemical quenching of fluorescence in terms of the maximum and minimum quantum yields, $\phi_{f_{\max}}$ and $\phi_{f_{\min}}$, and the fraction of open PSII reaction centers, A .

$$\phi_f = \phi_{f_{\min}} A + \phi_{f_{\max}} (1 - A) \quad (1)$$

Using target theory, A was expressed in terms of the irradiance, E_o , and the irradiance where photosynthesis is noticeably saturated from the instantaneous photosynthesis irradiance curve, E_k (Falkowski and Kiefer 1985).

$$A = e^{-E_o/E_k} \quad (2)$$

Kiefer and Reynolds set the values of $\phi_{f_{\min}}$ and $\phi_{f_{\max}}$ to 0.02 and 0.05, respectively, and adjusted the single step probabilities to match.

Nonphotochemical quenching, q_N , that not related to photochemistry, involves processes that dissipate excess irradiance as a mechanism to prevent photo-oxidative damage (Krause and Weis 1991; Demmig-Adams and Adams 1992; Horton et al. 1996). Nonphotochemical quenching appears to operate over longer timescales than photochemical quenching and involves a number of processes with varying induction and relaxation times. Energy-dependent quench-

ing, q_E , describes thermal dissipation of excitation energy in the pigment antenna associated with the cycling of xanthophyll pigments (Demmig-Adams 1990) and regulation of a chlorophyll-binding protein with rapid induction and relaxation kinetics (Li et al. 2000). q_E is brought on by the light-driven pH gradient across the thylakoid membrane. Quenching associated with state transitions, q_T , is normally small (Krause and Weis 1991) but may account for up to 20% of the changes in the absorption of PSII in aquatic environments (Falkowski and Raven 1997). Increased light stress leads to quenching associated with the photoinhibition of photosynthesis, q_I , with relaxation occurring on much longer timescales, and may be associated with protective energy dissipation and/or PSII reaction center damage (Horton et al. 1996). Nonphotochemical quenching is evident as a diel periodicity of in vivo fluorescence near the surface, with q_N decreasing the fluorescence in the middle of the day (Kiefer 1973; Falkowski and Kolber 1995; Dandonneau and Neveux 1997; Marra 1997; Kinkade et al. 1999). Kiefer and Reynolds (1992) noted that nonphotochemical quenching began near values of irradiance for the onset of saturation of photosynthesis. Babin et al. (1996) expanded the Kiefer and Reynolds model to include nonphotochemical quenching.

The use of sun-stimulated fluorescence to predict phytoplankton biomass and primary production has been based on two conflicting paradigms. To use it as a measure of biomass the quantum yield of fluorescence should remain constant, whereas, for determining the photosynthetic rate, the quantum yield of fluorescence should not only vary but vary in a deterministic manner with the photochemical yield. To understand the applicability of fluorescence measurements, sources of variability of the fluorescence quantum yield must be understood. The present article presents vertical profiles of ϕ_f derived from a simple algorithm that accounts for Raman and elastic scattering. This approach is used to study the quenching of chlorophyll fluorescence in natural systems, and an irradiance-based fluorescence quenching model is presented. The algorithm also has the potential to be directly applied to data collected by satellite-based sensors.

Theoretical background

Fluorescence of Chl a—The light reemitted as fluorescence from phytoplankton in a unit volume of water or fluorescence output, F_f , is determined by the absorbed flux and the quantum yield of fluorescence, ϕ_f . Excitation energy for phytoplankton occurs over a distinct spectral range, ~400–700 nm, often termed the photosynthetically available radiation (PAR). The absorbed flux at a given depth, z , can be calculated using the spectrally weighted phytoplankton absorption coefficient, \bar{a}_{ph} , and the integral of the scalar irradiance over this spectral region, $E_o(\text{PAR})$.

$$F_f(z) = \phi_f(z) \bar{a}_{ph}(z) E_o(\text{PAR}, z) \quad (3)$$

The spectrally weighted phytoplankton absorption coefficient is calculated using Eq. 4.

$$\bar{a}_{\text{ph}}(z) = \frac{\int_{\lambda=400}^{700} a_{\text{ph}}(\lambda, z) E_o(\lambda, z) d\lambda}{\int_{\lambda=400}^{700} E_o(\lambda, z) d\lambda} \quad (4)$$

Reabsorption of fluoresced light within the cells means that the quantum yield of fluorescence described in Eq. 3 and hereafter is a realized or measured yield and differs from the true physiological yield (Maritorena et al. 2000).

The spectral nature of the fluorescence emission can be approximated by a Gaussian emission function with a peak at λ_0 and standard deviation σ_f (Mobley 1994).

$$\frac{F_f(\lambda)}{F_f} = \frac{1}{2\sqrt{2\pi}\sigma_f} \exp\left[-\frac{(\lambda - \lambda_0)^2}{2\sigma_f^2}\right] = F_f^-(\lambda, \lambda_0, \sigma_f) \quad (5)$$

Given λ_0 and σ_f , it is therefore possible to calculate the ratio of the fluorescence emission at a single wavelength to the total emission, $F_f^-(\lambda, \lambda_0, \sigma_f)$, and to estimate the total fluoresced flux from a fluorescence emission determined at one wavelength. The measurement of $F_f(\lambda)$ at two wavelengths, λ_1 and λ_2 , allows the estimation of the standard deviation of the emission function if λ_0 is known.

$$\sigma_f = \sqrt{\frac{(\lambda_2 - \lambda_0)^2 - (\lambda_1 - \lambda_0)^2}{2 \ln\left(\frac{F_f(\lambda_1)}{F_f(\lambda_2)}\right)}} \quad (6)$$

The upwelling nadir radiance from fluorescence, L_{uf} , at a sensor may be expressed in terms of the fluorescence emission per unit volume under the assumption of an isotropic fluorescence emission and a homogeneous water column below the sensor (Kiefer et al. 1989).

$$L_{\text{uf}}(\lambda, z) = \frac{1}{4\pi} \frac{F_f(\lambda, z)}{[K_o(\text{PAR}, z) + a(\lambda, z)]} \quad (7)$$

The decrease in both the excitation energy and the fluorescence emission reaching the sensor are accounted for using the attenuation coefficient of the scalar PAR irradiance, $K_o(\text{PAR})$, and the total absorption coefficient, $a(\lambda)$, respectively.

Combining Eqs. 3, 5, and 7, it is possible to derive an expression for ϕ_f .

$$\phi_f(z) = 4\pi \frac{L_{\text{uf}}(\lambda, z) F_f^-(\lambda, \lambda_0, \sigma_f) [K_o(\text{PAR}, z) + a(\lambda, z)]}{\bar{a}_{\text{ph}}(z) E_o(\text{PAR}, z)} \quad (8)$$

Raman scattering of light by water—A model of Raman scattering was developed on the basis of the relationships of Walrafen (1967, 1969) as detailed in Mobley (1994) and errata (Mobley, pers. comm.). Excitation wavelengths of importance to scattering to the range of Chl *a* fluorescence output range from 510 to 600 nm. The total upwelling light due to Raman scattering, $L_{\text{ur}}(\lambda)$, can be approximated using similar arguments to those used for fluorescence by Chl *a*.

$$L_{\text{ur}}(\lambda_{\text{em}}, z) = \frac{1}{4\pi} \frac{\int_{\lambda_{\text{ex}}=i}^j E_o(\lambda_{\text{ex}}, z) b_R(\lambda_{\text{ex}} \rightarrow \lambda_{\text{em}}) d\lambda}{[K_o(\lambda_{\text{ex}}, z) + a(\lambda_{\text{em}}, z)]} \quad (9)$$

The $\frac{1}{4}\pi$ accounts for the contribution of total Raman scattering to upwelling radiance with an assumed isotropic emission resulting from diffuse excitation (Marshall and Smith 1990). $b_R(\lambda_{\text{ex}} \rightarrow \lambda_{\text{em}})$, the Raman scattering coefficient from the excitation to the emission wavelength, is the product of $a_R(\lambda)$, the Raman absorption coefficient, and $f^R(\lambda_{\text{ex}} \rightarrow \lambda_{\text{em}})$, the Raman wavelength distribution function.

Methods

Cruises and measurements—The Malin Shelf Break off the North Eastern Coast of the United Kingdom was visited during two cruises timed to coincide with the spring phytoplankton increase during 1995 (CD93) and 1996 (CH126) as part of the Land Ocean Interaction Study (LOIS) Shelf Edge Study. Optical casts, which consisted of paired spectroradiometer and conductivity-temperature-depth (CTD) profiles, were performed at a variety of locations between 56.2 and 57.0°N and 8.5 and 10.0°W during these cruises, with water depths from 200 to 2000 m. A PRR-600 underwater radiometer (Biospherical Instruments) with wavelengths designed to match those of the SeaWiFS sensor (downwelling irradiance, E_d [412, 443, 490, 510, 555, and 665 nm and PAR], upwelling radiance, L_u [412, 443, 490, 510, 555, 665, and 683 nm] and 10 nm half-maximum bandwidth) was used to determine the distribution of the underwater light field. Processing of radiometer casts was performed using methods similar to those described in Siegel et al. (1995), and the data were averaged to 1-m bins. Discrete water samples, taken during the CTD cast, were analyzed for optically important constituents. The Chl *a* concentration was measured using a Turner Designs Model 10 fluorometer previously calibrated using a Chl *a* pigment standard (Sigma Chemical Co.) (Tett 1987). Shimadzu UV-1201 and UV-1601 spectrophotometers were used during CD93 and CH126, respectively, to determine particulate absorption, $a_p(\lambda)$, and absorption by CDOM, $a_{\text{CDOM}}(\lambda)$, between 350 and 750 nm. The $a_p(\lambda)$ measurements were made using the quantitative filter technique (QFT) (Yentsch 1962; Mitchell 1990) with samples filtered on Whatman GF/F filters; a wetted filter was used as a blank, and optical densities were corrected using the path-length amplification correction of Cleveland and Weidemann (1993). The absorption by a_{CDOM} was determined using water filtered through a 0.2- μm Nucleopore filter and analyzed in a 10-cm quartz cuvette with a pure water standard in a matched reference cuvette.

Particulate absorption spectra were decomposed into absorption due to phytoplankton, $a_{\text{ph}}(\lambda)$ and nonalgal particulate matter, $a_d(\lambda)$, using an iterative fitting method similar to that described in Hoepffner and Sathyendranath (1993). This was based on the assumptions that phytoplankton absorption could be modeled by the product of the chlorophyll concentration, C , and the chlorophyll-specific phytoplankton absorption coefficient, a_{ph}^* and that nonalgal absorption decreased exponentially with increasing wavelength with slope S .

$$a_p(\lambda) = C a_{\text{ph}}^*(\lambda) + a_d(\lambda_0) e^{-S(\lambda - \lambda_0)} \quad (10)$$

The spectral chlorophyll-specific phytoplankton absorption coefficient used for the decomposition was derived from

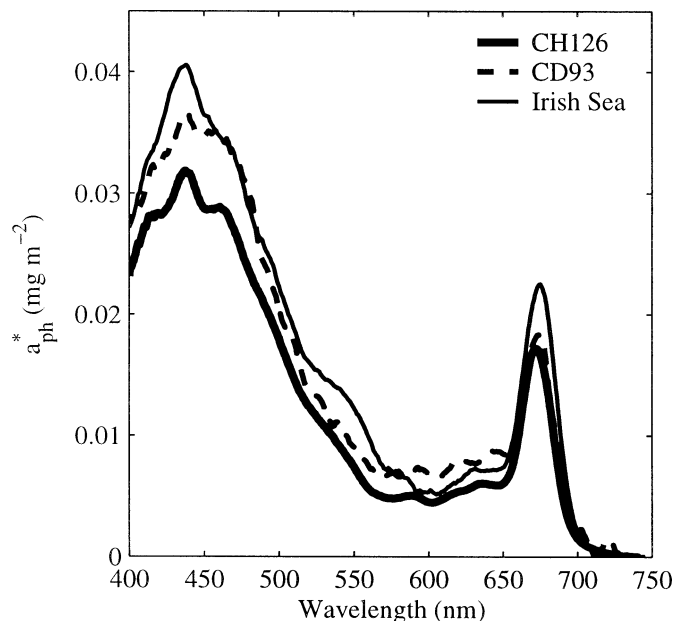


Fig. 1. The Chl *a*-specific phytoplankton absorption coefficient spectra, $a_{ph}^*(\lambda)$, used in the study. The Irish Sea spectrum was used in the initial mathematical a_p decomposition. The mean a_{ph}^* was calculated for both cruises, CH126 and CD93, and these were used in the reflectance inversion.

measurements made in the Irish Sea, where a_d did not covary with a_{ph} (Fig. 1). Under these conditions, linear regression of the $a_p(\lambda)$ against the chlorophyll concentrations yields $a_{ph}^*(\lambda)$ and the mean $a_d(\lambda)$. The modeled particulate absorption spectra were fitted to observed spectra by iteratively adjusting C , $a_d(\lambda_0)$, and S to minimize the sum of square deviations between the spectra. Phytoplankton absorption spectra were calculated from the difference between $a_p(\lambda)$ and $a_d(\lambda)$, which allowed the spectral shape of a_{ph} to vary from the initial a_{ph}^* . This can be seen in the mean $a_{ph}^*(\lambda)$ calculated for each cruise (Fig. 1).

Algorithm development—The algorithm to calculate ϕ_f consists of three main steps: (1) inversion of the measured radiance reflectance, L_u/E_d , using the five wavelengths below 600 nm to obtain inherent optical properties (IOPs); (2) decomposition of the upwelling radiance at 665 and 683 nm into that from fluorescence, backscattered light, and Raman scattering; and (3) calculation of ϕ_f from a combination of measured and retrieved parameters.

Inversion of the radiance reflectance—The Garver and Siegel (1997) method for inverting the remote sensing reflectance of water, measured at discrete wavelengths unaffected by inelastic scattering processes, was used to give the inherent optical properties, phytoplankton absorption, a_{ph} , absorption by nonalgal matter including CDOM and nonalgal particles, a_{dm} , and particulate backscatter, b_{bp} . The radiance reflectance is used in the present study, because it is analogous to the remote sensing reflectance, R_{rs} . The method is based on three main assumptions, that (1) there is a relationship between the remote sensing reflectance and the

total absorption and backscattering coefficients, (2) the inherent optical properties of pure water are well known, and (3) the spectral shapes of the specific absorption coefficients, a_{ph}^* and a_{dm}^* , and the specific particulate backscattering coefficient, b_{bp}^* , are well characterized. The semianalytical relationship for the remote sensing reflectance, R_{rs} , of Gordon et al. (1988) is used in the inversion

$$R_{rs}(\lambda) \equiv \frac{L_u(\lambda)}{E_d(\lambda)} \equiv \sum_{i=1}^2 l_i \left[\frac{b_b(\lambda)}{b_b(\lambda) + a(\lambda)} \right]^i \quad (11)$$

where $l_1 = 0.0949$ and $l_2 = 0.0794$.

In the present study, the total absorption coefficient was calculated as the sum of the constituent coefficients: the absorptions by water, $a_w(\lambda)$, phytoplankton, $a_{ph}(\lambda)$, and nonalgal matter, $a_{dm}(\lambda)$. The absorption coefficients of pure water were taken from Pope and Fry (1997). Absorption by nonalgal matter was represented by an exponential function with slope S and reference wavelength ($\lambda_0 = 440$ nm) (Bricaud et al. 1981). The absorption due to phytoplankton was calculated from the product of the Chl *a* concentration, C , and the chlorophyll-specific phytoplankton absorption coefficient. Total absorption was then calculated using Eq. 12.

$$a(\lambda) = a_w(\lambda) + a_{dm}(\lambda_0)e^{-S(\lambda-\lambda_0)} + Ca_{ph}^*(\lambda) \quad (12)$$

Similarly, the total backscattering coefficient was calculated from the sum of the constituent coefficients. The scattering coefficient for seawater, b_w , was modeled with a value at a reference wavelength and a $\lambda^{-4.32}$ spectral dependence (Morel 1974; Haltrin and Kattawar 1991). Backscattering by water was assumed to be half the total scattering. Particulate backscattering was modeled using an inverse power function of the wavelength as in Garver and Siegel (1997). The total backscattering was then calculated using Eq. 13.

$$b_b(\lambda) = \frac{1}{2}7.55 \times 10^{-3} \left(\frac{400}{\lambda} \right)^{4.32} + b_{bp}(\lambda_0) \left(\frac{\lambda}{\lambda_0} \right)^{-n} \quad (13)$$

Thus, in calculating a modeled L_u/E_d spectra (using Eqs. 11–13), there are six unknowns: three tuning parameters, S , n , and $a_{ph}^*(\lambda)$; and three retrieved parameters, C , $a_{dm}(\lambda_0)$, and $b_{bp}(\lambda_0)$. Profiles of the retrieved parameters were obtained by iteratively varying C , $a_{dm}(\lambda_0)$, and $b_{bp}(\lambda_0)$ to minimize the sum of squared deviations between modeled and observed L_u/E_d spectra below 600 nm. At these wavelengths, the effects of inelastic sources on the upwelling radiance were minimal compared with those at wavelengths >600 nm.

The tuning parameters were adjusted for each cruise to maximize the fit of the retrieved parameters to observed values. Three criteria were used to locally tune the inversion model: (1) the root mean square (RMS) error between observed and predicted reflectances at 5 m for each profile, (2) the relationship of the observed (using QFT decomposition) and predicted a_{ph} , and (3) the number of retrieved $a_{dm}(\lambda) < 0$ (retrieved values were not limited in range). For this, the values 0.010, 0.015, and 0.020 nm^{-1} were used for S , and 0, 1, and 2 were used for n . The mean a_{ph}^* spectra for each cruise and that from the Irish Sea described previously was used (Fig. 1). Only those measured reflectance spectra where the coefficient of variation of the surface irradiance was $<5\%$, the tilt and roll were $<10^\circ$, and the solar zenith angle

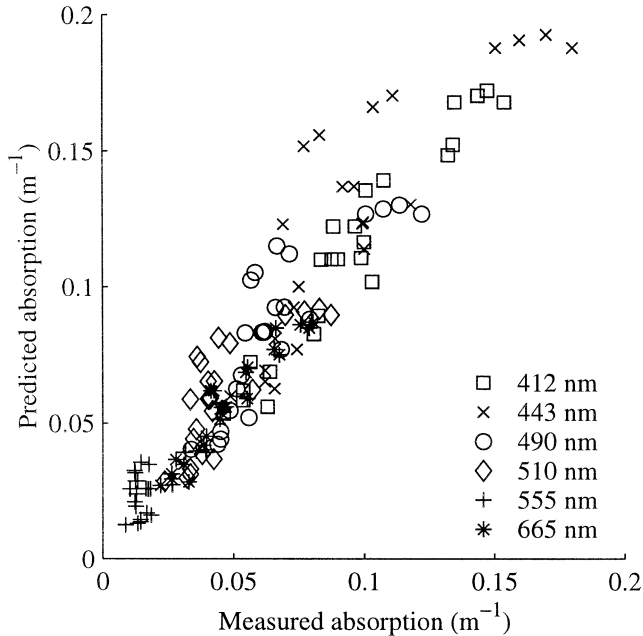


Fig. 2. Predicted and observed phytoplankton absorption for CH126. There was a significant relationship between observed and predicted values at all wavelengths, and all except 555 nm had a slope not significantly different from one (overall $r^2 = 0.90$).

were $<65^\circ$ were considered. The spectral shapes and the constituent concentrations from the reflectance inversion were then used to predict the IOPs and radiance reflectances at wavelengths other than those used for the inversion.

Decomposition of the upwelling radiance above 600 nm—There are three major sources for upwelling radiance at wavelengths where Chl *a* fluorescence is important, elastic scattering of ambient solar radiation of the same wavelength, and the inelastic inputs of Raman scattering and Chl *a* fluorescence. To obtain the upwelling radiance from fluorescence, it is therefore necessary to quantify the radiance from elastic and Raman scattering so that these can be subtracted from the total upwelling radiance.

Elastic scattered upwelling radiance at 665 nm was calculated using the modeled reflectance and the measured downwelling irradiance (Eq. 11). At 683 nm this was more complicated, because there was no $E_d(683)$ sensor. Instead, $E_d(683)$ was modeled. For a homogeneous ocean in the absence of inelastic scattering, the downwelling irradiance at one wavelength may be approximated from another using the differences in the attenuation and an exponential decrease with depth.

$$E_d(\lambda, z) = \gamma(\lambda_0, \lambda, 0^+) E_d(\lambda_0, z) e^{(K_d(\lambda_0) - K_d(\lambda))z} \quad (14)$$

The use of Eq. 14 allows for a more robust estimation of $E_d(\lambda, z)$ compared with simply extrapolating a surface measurement to depth.

Not considering Fraunhofer lines, $\gamma(\lambda_0, \lambda, 0^+)$, the ratio of surface irradiances was approximated using λ_0/λ at wavelengths >500 nm (Bird 1984). To predict the irradiance at depth, the difference in the attenuation coefficients $K_d(\lambda)$ and $K_d(\lambda_0)$, unaffected by inelastic scattering, was required. The

coefficients were calculated with the empirical relationship of Kirk (1991) using the extrapolated IOPs from the reflectance inversion and total scattering estimated using a backscattering ratio of 0.019. The cosine of the refracted solar zenith angle, μ_{sw} , and the mean cosine of scattering, g , were used in this relationship. The values of the backscattering ratio and the mean cosine of scattering, 0.924, were from the volume scattering function of (Petzold 1972).

$$\bar{K}_d(\lambda) = \frac{a(\lambda)}{\mu_{sw}} \left[1 + G(\mu_{sw}, g) \frac{b(\lambda)}{a(\lambda)} \right]^{0.5} \quad (15)$$

$$G(\mu_{sw}, g) = \mu_{sw} \left(\frac{2.236}{g} - 2.447 \right) - \left(\frac{0.849}{g} - 0.739 \right) \quad (16)$$

The modeled downwelling irradiance at 683 nm was then used to estimate the upwelling radiance using the measured $E_d(665)$, the predicted radiance reflectance and attenuation coefficients. This method was also used to assess the contribution of inelastic sources to the downwelling irradiance at 665 nm using the measured $E_d(555)$.

The proportion of the upwelling radiance due to Raman scattering was calculated for both 665 and 683 nm (Eq. 9). The integral was calculated using measured $E_d(\lambda)$ data interpolated at 1 nm resolution. The observed $K_d(555, z)$ was used to give the attenuation of the exciting radiation because this was at the center of the excitation range and $a(\lambda_{em}, z)$ from the modeled absorption.

Fluorescence output and quantum yield—The fluorescence output was calculated at each depth for all profiles using Eq. 7 at both 665 and 683 nm using the observed $K_d(\text{PAR}, z)$ as an approximation for $K_d(\text{PAR}, z)$ and the extrapolated $a(\lambda, z)$ value from the reflectance inversion. Equation 6 was used to obtain σ_f , and the mean value for each cruise was used to estimate $F_f^-(683, 683, \sigma_f)$. This, combined with the $F_f(683, z)$, gave the total fluorescence emission per unit volume for each depth (Eq. 5).

The spectrally weighted absorption was calculated using the measured $E_d(\lambda, z)$ interpolated from 400 to 700 nm and the $a_{ph}(\lambda, z)$ from both the QFT measurements and the reflectance inversion (Eq. 4). Finally, $\phi_f(z)$ was calculated using the scalar PAR irradiance, estimated from $E_d(\text{PAR}, z)/\mu_{sw}$, as described above (Eq. 3).

Results

Inversion of the radiance reflectance—There were significant linear relationships between the observed a_{ph} and those predicted by reflectance inversion for all values of the tuning parameters. The particulate backscattering exponent, n , and the spectral shape of the specific phytoplankton absorption, $a_{ph}^*(\lambda)$, were found to give the greatest variability in the inversion. For data from the 1996 cruise, the inversion performed best with the cruise mean a_{ph}^* , an n of 2, and S of 0.010 nm^{-1} . With these values the RMS error was minimal, observed and predicted phytoplankton absorptions were closest to a 1:1 relationship (overall $r^2 = 0.90$), and no a_{dm} values were <0 (Fig. 2). The parameterization of the tuning factors for 1995 data set was not as simple. All values of n

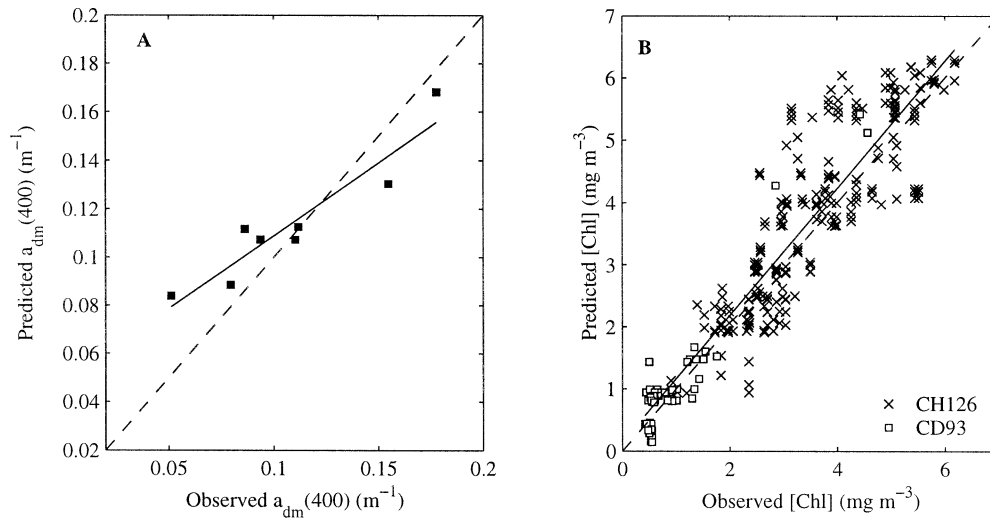


Fig. 3. Retrieval of nontuning parameters. (A) Nonalgal absorption, a_{dm} . Observations of nonalgal absorption that had associated optical measurements were limited to 8. These were close to a 1:1 relationship ($a_{dm}^{pred} = 0.60a_{dm}^{obs} + 0.05$, $r^2 = 0.88$). (B) Chlorophyll concentration (Chl). Comparison of the observed and predicted chlorophyll concentrations from both CH126 and CD93 showed that there was a significant relationship between the two that was not significantly different from 1:1 ($C^{pred} = 1.02C^{obs} + 0.15$, $r^2 = 0.84$). For both panels, the dashed line is 1:1 and the solid line represents the best fit to the data.

led to an overestimation of a_{ph} . The three optical casts with the maximum phytoplankton absorption (6, 8, and 10) affected the results strongly and were all located at the same station. Comparison between the chlorophyll concentrations determined fluorometrically from extracts of the QFT absorption filter and the 250-ml samples for cast 8 suggested that phytoplankton absorption may have been underestimated by a factor of 1.7. This was potentially due to errors in filtering and/or patchiness in the phytoplankton distribution. Adjusting for this error, the values for n of 1 and S of 0.010 nm^{-1} and the cruise mean $a_{ph}^*(\lambda)$ were used, because these represented a compromise of the optimal values of the three tuning criteria. For both cruises, there was no discernable trend in the RMS error of the reflectance inversion with depth.

The performance of the reflectance inversion was assessed using observations that were not used to tune the model, nonalgal absorption, and chlorophyll concentration. Nonalgal absorption was composed of that from both particulate organic matter and CDOM. Particulate nonalgal absorption estimates from the a_p decomposition method were combined with direct measurements of the a_{CDOM} to give a_{dm} . Only eight direct measurements of a_{CDOM} were concurrent with quality checked in-water optical measurements, and were all from CH126. There was a significant relationship between the predicted and the observed $a_{dm}(400)$ values that was close to a 1:1 relationship ($r^2 = 0.88$, Fig. 3A). During CH126 and CD93, respectively, 246 and 51 in-water optical measurements that passed quality criteria had associated fluorometrically determined chlorophyll concentrations. There was a significant relationship between the observed and predicted chlorophyll values that was not significantly different from a 1:1 relationship ($r^2 = 0.84$, Fig. 3B). There was no discernable trend in the RMS error of the chlorophyll

relationship with depth. Reflectance inversion is generally used in surface waters where the quasi single scattering approximation may be assumed to hold. The lack of discernable trends in the RMS error of the reflectance inversion and the chlorophyll relationship suggests that the inversion is valid for the profiles used in the present study.

Effects of inelastic sources at 665 and 683 nm—There was a significant relationship between the $K_d(443)$ calculated using the retrieved IOPs and those observed with the PRR-600 ($r^2 = 0.74$, Fig. 4). This was close to a 1:1 relationship. In contrast, the observed values of $K_d(665)$ differed significantly from the modeled values and showed a marked decrease with depth unlike those at other wavelengths (Fig. 5A). The most probable reason for this was the contribution of inelastically scattered light. To determine this, the $E_d(555)$ was used to predict $E_d(665)$ in the absence of inelastic scatter (Eq. 14). The difference between the calculated and observed $E_d(665)$ profiles allowed the calculation of the effect of inelastic sources (Fig. 5B). The contribution of inelastic processes was also determined from the predicted and observed attenuation coefficients (using the ratio of the difference between observed K_d at 555 and 665 nm and the difference between the observed $K_d[555]$ and predicted $K_d[665]$).

The composition of the upwelling radiance at 665 nm showed a characteristic distribution: the backscattered light, $L_{ub}(665)$, decreased exponentially with depth as $E_d(665)$ was rapidly absorbed; the influence of the Raman scattered light, $L_{ur}(665)$, increased with depth as light redistributed from other wavelengths became more important; and the contribution from upwelled fluorescence, $L_{uf}(665)$, also increased with depth (Fig. 6A, Table 2). The distribution for the contribution of the components of total upwelled radiance at 683

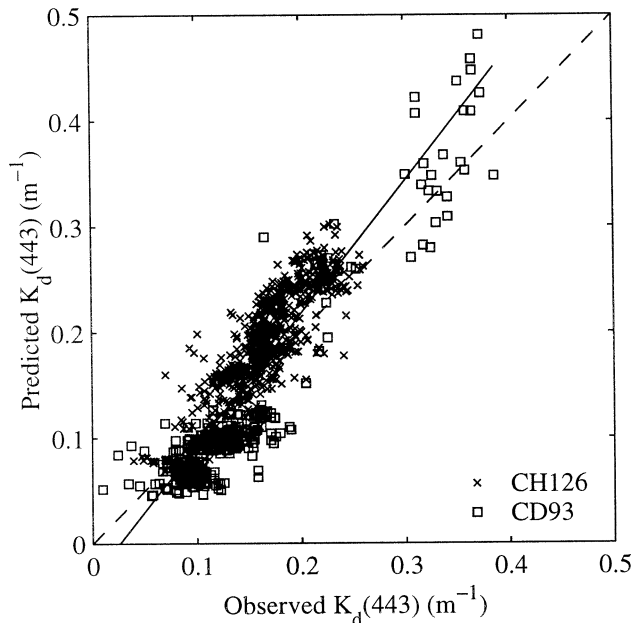


Fig. 4. Predicted and observed attenuation coefficients at 443 nm. The predicted $K_d(443)$ were calculated using IOPs retrieved from the reflectance inversion and the relationship of Kirk (1991, Eqs. 15 and 16). There was a significant relationship between the two that was close to 1:1 ($K_d^{\text{pred}}[443] = 1.25K_d^{\text{obs}}[443] - 0.03$, $r^2 = 0.80$). The dashed line is 1:1, and the solid line represents the best fit to the data.

nm was similar to that for 665 nm (Fig. 6B, Table 2). Comparison of compositions at the two wavelengths showed the lesser magnitude of the influences of both back and Raman scattered light at 683 nm because of the increased amount of inelastic scattering from fluorescence.

Fluorescence output and quantum yield—Below 5 m, the fluorescence outputs at 665 and 683 nm were significantly related for both cruises ($r^2 > 0.99$). The mean standard deviations of the Gaussian emission function for each cruise, calculated from the ratio of the fluorescence outputs, were close to the 10.6 nm historically reported (Gordon 1979; Kishino et al. 1984). The σ_f were $11.58 (\pm 0.60)$ and $10.53 (\pm 0.45)$ nm for CH126 and CD93, respectively. Above 5 m, nonfluorescence components dominated $L_u(665)$, and their overestimation caused the fluorescence signal to be undetected or underestimated in some cases. At 683 nm the increased fluorescence signal, compared with the nonfluorescent sources of a similar magnitude at 665 nm, meant that similar potential errors were greatly reduced.

Spectrally weighted absorption was calculated using values of phytoplankton absorption obtained from both the reflectance inversion and QFT (Eq. 4). There was a strong agreement between the two values ($r^2 = 0.83$, Fig. 7A). The quantum yield of fluorescence calculated from both estimates of \bar{a}_{ph} again showed a significant relationship for both cruises that was not significantly different from a 1:1 relationship ($r^2 = 0.86$, Fig. 7B). All of the estimates of ϕ_f from just the radiometric measurements were within $\pm 40\%$ of those obtained by incorporating QFT measurements, which

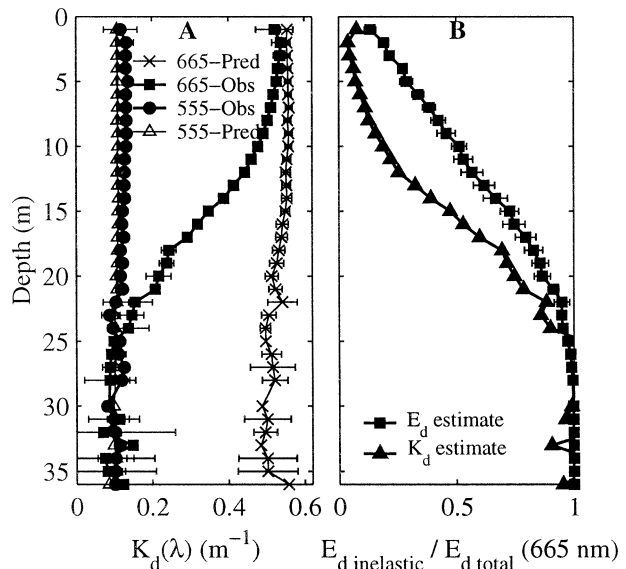


Fig. 5. The effect of inelastic scattering on $E_d(665)$. (A) The observed $K_d(665)$ showed a marked decrease with depth unlike values predicted from retrieved IOPs and the Kirk (1991) algorithm and $K_d(555)$. This was due to the increasing contribution of inelastic scattering sources. (B) The contribution of inelastic scattering to $E_d(665)$ was calculated in two ways. First, using Eq. 14 and the observed $E_d(555)$ and, second, from the mean predicted and observed attenuation coefficients using $(K_d^{\text{obs}}[555] - K_d^{\text{obs}}[665]) / (K_d^{\text{obs}}[555] - K_d^{\text{pred}}[665])$. Both estimates clearly show an increase in the inelastic contribution with depth to 25 m when virtually all $E_d(665)$ is from inelastic sources. For both panels the 95% confidence intervals are represented by the horizontal bars. Where no bars are apparent, the interval was smaller than the size of the marker, except the K_d estimate of the inelastic contribution, for which no confidence interval was calculated.

indicates that ϕ_f can be reasonably estimated from radiometric measurements alone.

Sources of variability in the fluorescence signal—The fluorescence output is determined by the incident irradiance, the phytoplankton absorption, and the quantum yield of fluorescence (Eq. 3). Of interest is partitioning the variability of the fluorescence output among these three factors, because this determines what can be implied from changes in measured phytoplankton fluorescence. After logarithmic transformation, the fluorescence and exciting irradiance were significantly related with 86% of the variance in the fluorescence output being explained by the irradiance. The slope of the regression, which corresponds to an exponent of the irradiance without the logarithmic transformation, was not significantly different from 1 ($P = 0.14$, $n = 1001$), which could allow F_f to be estimated from a simple ratio of $E_o(\text{PAR})$. The relationship was $F_f = 8.77 \times 10^{-4} E_o(\text{PAR})$. Historically, the variability associated with the irradiance has been removed by normalizing the fluorescence output by the exciting irradiance. Linear regression showed that 56% of the variability of this irradiance normalized fluorescence, often termed the fluorescent coefficient, was explained by spectrally weighted absorption coefficient. This is the relationship that has been used to predict biomass from solar-

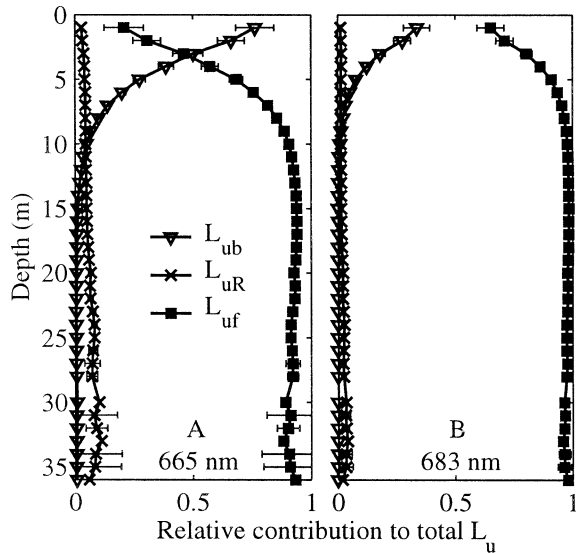


Fig. 6. The mean composition of upwelling radiance for (A) 665 and (B) 683 nm during CH126. The vertical bars indicate the 95% confidence interval. The effect of Raman scattering, $L_{ur}(\lambda)$, varied least with a steady increase with depth at both wavelengths. The contribution of backscattered light, $L_{ub}(\lambda)$, decreased rapidly with depth at both wavelengths, and fluoresced light, $L_{uf}(\lambda)$, comes to dominate with depth. The upwelled radiance over the fluorescence band was never fully composed of that from fluorescence at any depth due to Raman scattered light, which always formed a significant proportion.

stimulated fluorescence. A simple model for ϕ_f is an exponential decrease with increasing irradiance similar to the nonphotochemical quenching model of Neale and Richerson (1987) and explained 29% of the variability of ϕ_f , such that $\phi_f = 0.032 \exp(1.32 \times 10^{-3} E_o[\text{PAR}])$. The exponent was similar to that of 1.22×10^{-3} reported by Neale and Richerson. Incorporating this model with the $F_f/E_o(\text{PAR})$ measurements allowed prediction of \bar{a}_{ph} , and 70% of the variability in the predicted \bar{a}_{ph} was explained by the observed values using linear regression, but the relationship was significantly different from 1:1 ($\bar{a}_{ph}^{\text{pred}} = 0.57\bar{a}_{ph}^{\text{obs}} + 0.14$).

Variability of the quantum yield of fluorescence—One concern with the method for calculating ϕ_f is the effect of a nonhomogeneous water column below the detector. Heterogeneity of the water column will have a differential effect

Table 1. Notation

Notation	
$a(\lambda), a_{ph}(\lambda), a_p(\lambda), a_d(\lambda), a_{dm}(\lambda), a_{CDOM}(\lambda), a_w(\lambda)$	Total absorption coefficient and those for phytoplankton, particulate, non-algal particulate, total non-algal, CDOM, and water (m^{-1})
$a_{ph}^*(\lambda)$	Chl <i>a</i> -specific phytoplankton absorption coefficient ($\text{m}^2 \text{mg Chl}^{-1}$)
$a_R(\lambda), b_R(\lambda_{ex} \rightarrow \lambda_{em})$	Raman absorption and scattering coefficients (m^{-1} and $\text{m}^{-1} \text{nm}^{-1}$)
$f^R(\lambda_{ex} \rightarrow \lambda_{em})$	Raman wavelength redistribution function (nm^{-1})
$b(\lambda), b_b(\lambda), b_p(\lambda), b_{bp}(\lambda)$	Total scattering coefficient and those for total backscatter, particulate scattering and particulate backscatter (m^{-1})
C	Chlorophyll concentration (mg m^{-3})
$E_d(\lambda), E_o(\lambda)$	Downwelling and scalar irradiances (W m^{-2} or $\mu\text{mol quanta m}^{-2} \text{s}^{-1}$)
E_k, E_T	Saturation irradiances for photosynthesis and energy dependant nonphotochemical quenching ($\mu\text{mol quanta m}^{-2} \text{s}^{-1}$)
$K_d(\lambda), K_o(\lambda)$	Downwelling and scalar diffuse attenuation coefficients (m^{-1})
$F_p, F_f(\lambda)$	Fluorescence emission per unit volume or fluorescence output ($\mu\text{mol quanta m}^{-3} \text{s}^{-1}$)
$F_f^*(\lambda, \lambda_o)$	Fluorescence emission ratio
ϕ_f	Quantum yield of fluorescence
g, μ_{sw}	Cosines of mean of scattering and refracted solar zenith angle
$L_u(\lambda), L_{ub}(\lambda), L_{ur}(\lambda), L_{uf}(\lambda)$	Upwelling radiance and that from elastic scattering, fluorescence, and Raman scattering ($\text{W m}^{-2} \text{sr}^{-1}$ or $\mu\text{mol quanta m}^{-2} \text{sr}^{-1} \text{s}^{-1}$)
R_{rs}	Remote sensing reflectance coefficient (sr^{-1})
A, r	Fraction of open and viable PSII reaction centers
n	Exponent of spectral particulate backscattering coefficient
S	Exponent coefficient of spectral CDOM or non-algal absorption coefficient (nm^{-1})
$\lambda_{ex}, \lambda_{em}$	Excitation and emission wavelengths (nm)
σ_f	Standard deviation of Gaussian fluorescence emission function (nm)
γ	Ratio of surface irradiances

Table 2. The mean percentage composition (standard deviation) of the total upwelling radiance at 665 and 683 nm for cruise CH126, represented graphically in Fig. 5.

Depth (m)	665 nm			683 nm			Number of observations
	L_{ub}	L_{ur}	L_{uf}	L_{ub}	L_{ur}	L_{uf}	
1	76.3 (18.7)	2.8 (1.2)	20.8 (19.2)	33.6 (12.8)	1.3 (0.6)	65.1 (13.2)	17
5	27.5 (10.4)	4.1 (1.4)	68.4 (11.4)	7.7 (3.6)	1.4 (0.6)	90.9 (4.2)	47
10	4.8 (1.3)	4.5 (1.4)	90.7 (2.5)	0.9 (0.3)	1.3 (0.5)	97.8 (0.7)	40
15	1.2 (0.2)	4.9 (1.1)	93.9 (1.2)	0.2 (0.0)	1.4 (0.3)	98.4 (0.4)	26
20	0.6 (0.1)	6.7 (1.9)	92.7 (1.8)	0.1 (0.0)	2.2 (0.6)	97.7 (0.6)	11
25	0.5 (0.0)	8.2 (0.0)	91.3 (0.0)	0.1 (0.0)	2.5 (0.0)	97.4 (0.0)	1
35	0.6 (0.1)	8.4 (3.8)	91.1 (3.9)	0.0 (0.0)	3.5 (1.0)	96.5 (1.0)	2

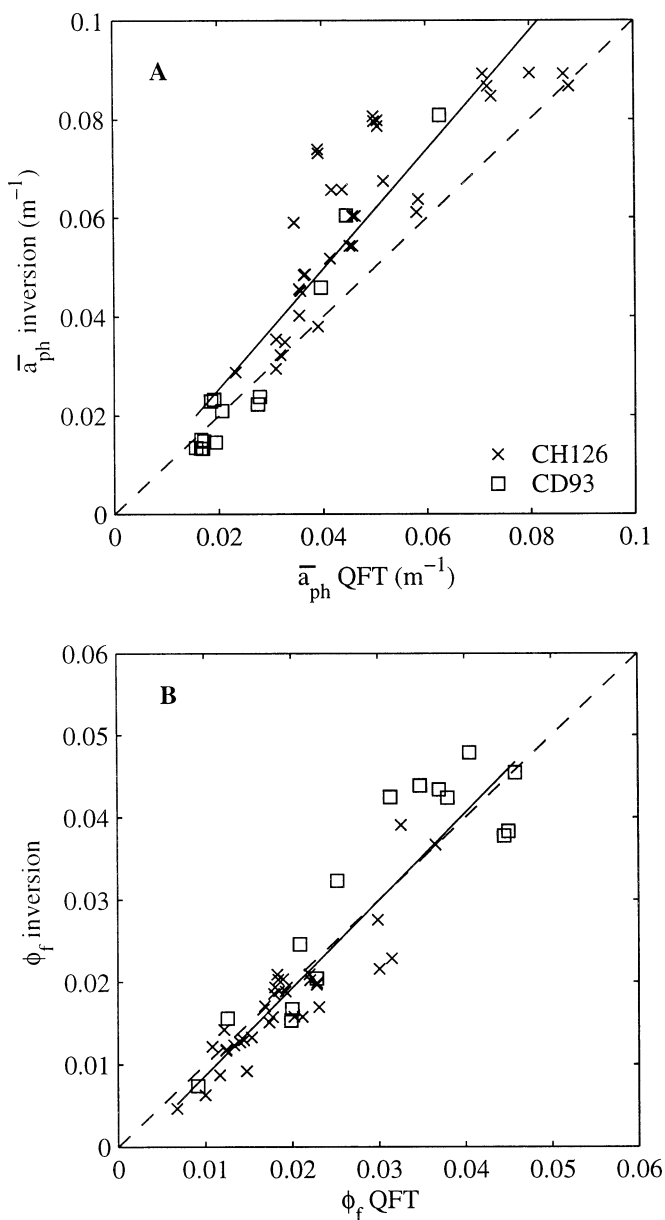


Fig. 7. (A) Spectrally weighted absorption, \bar{a}_{ph} , from direct QFT measurements and those from the reflectance inversion from both cruises. There was good agreement between the two ($\bar{a}_{ph}^{inv} = 1.21\bar{a}_{ph}^{QFT} + 0.00$, $r^2 = 0.83$). (B) The quantum yield of fluorescence, ϕ_f , calculated using absorptions from QFT measurements and those derived from the reflectance inversion for both cruises. There was a significant relationship between the two that was not significantly different from 1:1 ($\phi_f^{inv} = 1.06\phi_f^{QFT} + 0.00$, $r^2 = 0.86$). For both panels, the dashed line is 1:1 and the solid line represents the best fit to the data.

with wavelength, leading to inaccuracies in the retrieved inherent optical properties. For example, with a high-chlorophyll surface layer above lower chlorophyll waters, the change in the spectral quality of the upwelling light as the interface is approached may lead to an underestimation of \bar{a}_{ph} immediately above the boundary of the two waters. This would tend to raise the quantum yield of fluorescence. For

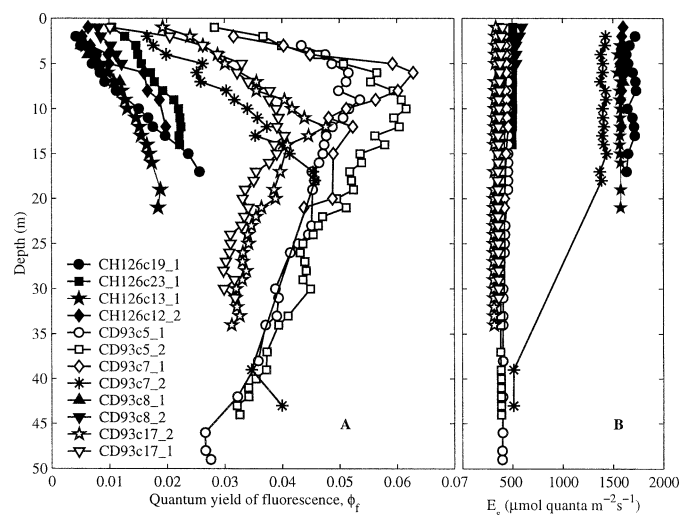


Fig. 8. Variation in the quantum yield of fluorescence with depth and surface irradiance. Two distinct regions were apparent in the variation of ϕ_f with depth: an increase from a low surface value to a subsurface maximum followed by a decrease with depth. Both regions were only present in casts before 1000 h local time (open symbols), which generally had low surface irradiance. Casts after 1000 h had depressed ϕ_f values compared with those earlier in the day, independent of surface irradiance conditions. The increase in ϕ_f to the subsurface maximum was indicative of decreased nonphotochemical quenching, whereas the decrease below the subsurface maximum indicated increasing photochemical quenching.

the discussion of the variability of ϕ_f below, the affect of this potential error was minimized by limiting the data to areas absent of sharp changes in biomass.

Two distinct regimes were observed in the variation of ϕ_f with depth and, hence, irradiance. An initial increase in the quantum yield with depth to a subsurface maximum was followed by a decrease with depth (Fig. 8, Table 3). The depth of the subsurface maximum was not constant and ranged from a minimum of 6 m during the first profile of cast 7 from CD93 to 18 m during the second profile of the same cast. After 1000 h local time, only the increase in ϕ_f with depth was observed. For the casts shown in Fig. 8, near-surface values of ϕ_f varied from 0.4% from midday, high-irradiance conditions of cast 19 of CH126 to 2.7% during the early morning, low light conditions of the cast 5 of CD93. The magnitude of ϕ_f at the subsurface maxima, where clearly discernable, ranged from 4.0% (profile 1 of cast 17 of CD93) to 6.3% (profile 1 of cast 7 from the same cruise). There is some evidence that ϕ_f from cast 13, profile 1, of CH126 reached a maximum at ~ 19 m of only 1.9%.

The two regimes of quantum yield of fluorescence were also discernable in the distribution with irradiance (Fig. 9, Table 3). Increasing irradiance initially led to an increase in the quantum yield of fluorescence to a maximum value between $E_o(PAR)$ values of 94 and 164 $\mu mol\ quanta\ m^{-2}\ s^{-1}$. Further increasing irradiance decreased the quantum yield of fluorescence to $\sim 0.5\%$ at irradiances around 2,000 $\mu mol\ quanta\ m^{-2}\ s^{-1}$. The inflection irradiance and the quantum yield at maximal irradiances appeared to be well conserved. Casts with large changes in the surface irradiance between

Table 3. Summary of observations for those casts in Figs. 8 and 9. The initial part of the legend indicates the cruise (either C126 or CD93), followed by the cast number and profile number, 1 or 2 indicating either a downcast or upcast, respectively. The surface irradiances, E_s , and the attenuation coefficients, K_d , are the mean for the profile. The depth and scalar irradiance, E_0 , are those for the maximum quantum yield of fluorescence, $\max(\phi_f)$, for each profile. The chlorophyll concentrations are the mean from fluorometric measurements for the top 30 m (standard deviation).

Legend	Cast	Profile	Time (h)	Date	$E_s(\text{PAR})$ ($\mu\text{mol quanta m}^{-2} \text{s}^{-1}$)	$K_d(\text{PAR})$ (m^{-1})	$\max(\phi_f)$	$E_0[\max(\phi_f)]$ ($\mu\text{mol quanta m}^{-2} \text{s}^{-1}$)	Depth (m)	$\min(\phi_f)$	Chl <i>a</i> (mg m^{-3})
c126c19_1	19	1	1048	7 May 96	1682.2	0.191	0.0257	91.0	17	0.004	3.95 (0.71)
c126c23_1	23	1	1230	10 May 96	502.9	0.154	0.0224	84.0	12	0.010	2.23 (0.59)
c126c13_1	13	1	1306	5 May 96	1569.9	0.171	0.0188	68.6	19	0.006	4.40 (0.91)
c126c12_2	12	2	1523	2 May 96	1595.4	0.142	0.0198	197.4	12	0.005	3.66 (0.51)
cd93c5_1	5	1			436.9	0.113	0.0536	164.0	9	0.027	
cd93c5_2		2	0851	11 May 95	384.6	0.110	0.0616	97.8	10	0.028	1.27 (0.18)
cd93c7_1	7	1			437.2	0.131	0.0629	145.2	6	0.032	
cd93c7_3		2	0900	12 May 95	1304.4	0.144	0.0457	122.3	18	0.017	1.53 (0.03)
cd93c8_1	8	1			1591.9	0.280	0.0119	267.5	7	0.005	
cd93c8_2		2	1040	15 May 95	556.5	0.318	0.0122	123.5	5	0.008	3.97 (1.32)
cd93c17_2	17	2			321.8	0.095	0.0476	94.0	12	0.019	
cd93c17_1		1	0809	28 May 95	366.8	0.099	0.0404	100.4	13	0.010	0.57 (0.08)

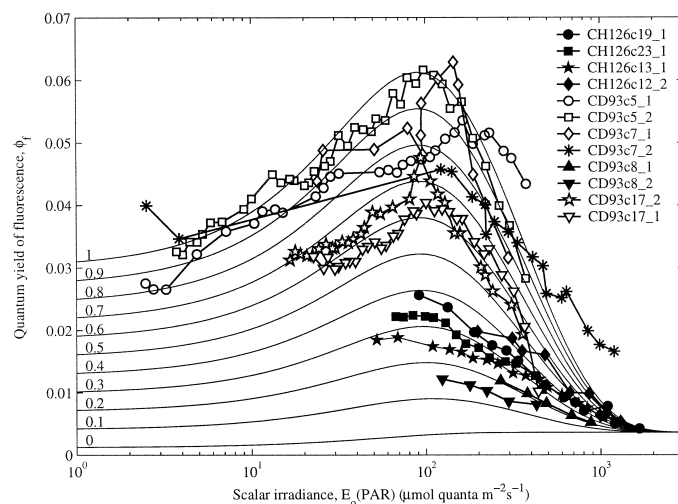


Fig. 9. Variation in the quantum yield of fluorescence with irradiance. The two regimes of variation in ϕ_f observed in Fig. 8 were apparent. Decreased photochemical quenching, from the closing of reaction centers, initially increased ϕ_f up to a maximum between 94 and 164 $\mu\text{mol quanta m}^{-2} \text{s}^{-1}$. Further increasing irradiance brought on nonphotochemical quenching and decreased ϕ_f . At high irradiances after 1000 h (closed symbols), the quantum efficiency at any given irradiance was suppressed compared to that before 1000 h. Short-term variations, <15 min, in irradiance did not greatly change the relationship of ϕ_f with irradiance, which indicates that physiological processes operating on two different timescales affected the fluorescence quantum efficiency. Short-term processes, <15 min, allowed ϕ_f to vary for a given photoadaptive state—that is, along the line for any given profile. Long-term processes changed the photoadaptive state, depressing the ϕ_f irradiance relationship. The numbers to the left and the lines below indicate the qI state and the model output described by Eq. 18.

successive profiles (cast 7 from CD93, where surface irradiance increased from 437 to 1,304 $\mu\text{mol quanta m}^{-2} \text{s}^{-1}$, and cast 8, where surface irradiance decreased from 1,592 to 556 $\mu\text{mol quanta m}^{-2} \text{s}^{-1}$) demonstrated that, although there may have been marked changes in the distribution of ϕ_f with depth for a single cast (Fig. 8), there was less marked change in the relationship with irradiance (Fig. 9).

Discussion

Reflectance inversion—This work has shown that, similar to previous work (e.g., Roesler and Perry 1995; Garver and Siegel 1997; O'Reilly et al. 1998), it is possible to use semi-analytical methods to invert remote sensing reflectances to give IOPs. The close agreement between $a_{\text{ph}}(\lambda)$ values retrieved from the inversion and those from QFT measurements on discrete water samples ($r^2 = 0.90$; Fig. 2) was expected, because this was one of the main factors used in tuning the inversion and was similar that reported by Roesler and Perry (1995). The close correspondence between retrieved and measured parameters not used in tuning, nonalgal absorption, and the Chl *a* concentration (Fig. 3) confirmed the functionality of the inversion algorithm. The degree of variability explained by the linear regression of the chlorophyll values ($r^2 = 0.81$) was similar to that re-

ported by Garver and Siegel (1997) and between high-performance liquid chromatography and fluorometric determinations of chlorophyll (author's unpubl. data). The functionality of the inversion was also confirmed by the close relationship between the observed attenuation coefficients and those modeled using the IOPs from the inversion—for example, the close relationship for modeled and observed $K_d(443)$ (Fig. 4) and the close agreement at the surface for $K_d(665)$ (Fig. 5A).

Composition of light at 665 and 683 nm—Inelastic sources of light have been shown to be a significant part of both downwelling and upwelling light fields. This was evident in the downwelling irradiance as a decrease in $K_d(665)$ with depth due to the rapid removal with depth of red light incident at the surface (Fig. 5A). Eventually, inelastic scattering dominated the light field and attenuation values reflected those at the excitation wavelengths. Light from inelastic sources formed a significant part of $E_d(665)$ even at shallow depths and by 10 m dominated the downwelling light field (Fig. 5B). This is in keeping with previous modeled (Marshall and Smith 1990; Berwald et al. 1998) and observed results (Maritorena et al. 2000). The dominance of inelastic sources with depth was also observed in the upwelling radiance (Fig. 6, Table 2). The contribution of Raman scattered light was significant and of a similar magnitude to previous studies (Haltrin and Kattawar 1991; Maritorena et al. 2000). Previous work has shown that chlorophyll fluorescence may only contribute on the order of 80% of the upwelling light field in the absence of elastically scattered light (Culver and Perry 1997). Because the maximal excitation wavelengths for the Raman scattering and Chl *a* fluorescence differ, it might be expected that the relative importance of these inelastic sources might vary. In locations where the optical properties allow maximal transmission of green light (around the 555 nm excitation peak of Raman scattering to 683 nm) and those with low phytoplankton biomass, Raman scattered light may come to dominate the light field at wavelengths of Chl *a* fluorescence. This raises the possibility of errors in previous measurements of natural fluorescence in which the only correction of the upwelling radiance was for backscattered light (Kiefer et al. 1989; Chamberlin et al. 1990; Chamberlin and Marra 1992; Kiefer and Reynolds 1992; Stegmann et al. 1992).

Although approximation allowed calculation of $E_d(683)$ from $E_d(665)$, including the effects of inelastic sources, it should be noted that the magnitude of the inelastic processes was for 665 nm. This potentially led to errors in both calculated $E_d(683)$ and $L_u(683)$. These errors would have been maximal where the effect of the inelastic sources was greatest—that is, with depth. Here the contribution of elastically scattered light would have been minimal, so the error in determining the fluorescence signal would have been minor. The use of an instrument with an $E_d(683)$ sensor would remove this potential source of error.

The fluorescence signal—The reflectance inversion algorithm was validated by direct comparison of retrieved parameters with independent measurements, but there were no independent measurements with which to validate the de-

composition algorithm for the upwelling radiance. Assessment of the decomposition was possible, however, by comparing the fluorescence output from the two channels, 665 and 683 nm. The strong linear agreement between the fluorescence output calculated from both channels ($r^2 > 0.98$), even at higher values associated with shallow depths and increased elastically scattered light, validated the decomposition algorithm. This was further confirmed by the close agreement between the calculated standard deviation of the Gaussian emission function and those previously reported (Gordon 1979; Kishino et al. 1984). The difference in the shapes of the fluorescence emission calculated for the two cruises may have been due to differences in instrument response and phytoplankton physiology. Spectral observations have shown the spectral shape of Chl *a* fluorescence varies under both natural and laboratory conditions (Prézelin and Ley 1980; Ahn et al. 1992; Roesler and Perry 1995) and models have suggested that changes in absorption efficiency of phytoplankton may alter the fluorescence output by means of internal reabsorption (Collins et al. 1985).

Values of ϕ_f calculated using the reflectance inversion and radiance decomposition algorithm and, hence, derived solely from in-water radiometer measurements, were not significantly different from values of ϕ_f calculated using QFT measurements of phytoplankton absorption ($r^2 = 0.86$, Fig. 7B). The reflectance inversion technique was limited to a single spectral shape for phytoplankton absorption for an individual tuning, in this case each cruise, and temporal and spatial variations in this shape may have explained the differences between the estimates of ϕ_f . Errors associated with QFT measurements of absorption, including sample preparation and assumptions inherent in the technique, specifically those associated with pathlength amplification factors, may have also contributed to the variance unexplained (Tassan and Ferrari 1995; Roesler 1998; Lohrenz 2000; Tassan et al. 2000).

The quantum yield of fluorescence—The ϕ_f depth profiles (Fig. 8) show many similarities to, but have shallower subsurface maxima than, those reported by Maritorena et al. (2000). Their depth profiles were from clear oligotrophic waters of the Pacific with lower $K_d(\text{PAR})$, 0.035–0.055 m^{-1} , allowing light to penetrate to greater depths. Simple calculations using reported surface irradiance levels, 1,600–2,000 $\mu\text{mol quanta m}^{-2} \text{s}^{-1}$, indicated that the ϕ_f maxima occurred at irradiances of similar magnitudes to those reported herein. The near-surface values of ϕ_f reported herein are also quantitatively similar to the 0.84% reported for the high irradiance conditions studied by Maritorena et al. (2000).

Three regions of control of the fluorescence yield of phytoplankton are observed in Fig. 9. First, at irradiances below that of inflection, increasing irradiance increases the fluorescence yield. Decreasing photochemical quenching, q_p , would explain this with increasing irradiance closing more reaction centers (Kiefer and Reynolds 1992). Second, above the inflection irradiance, further increasing irradiance decreases the fluorescence yield. Increasing nonphotochemical quenching would explain this, most likely the rapid energy-dependent quenching, q_E , because it appears to be rapidly variable. Last, after 1000 h, there is the general decrease in the mag-

nitude of the fluorescence yield at all irradiances, most probably explained by the long-timescale light-stress nonphotochemical quenching, q_I (Krause and Weis 1991; Demmig-Adams and Adams 1992; Horton et al. 1996).

A simple irradiance-based model that includes q_P , q_E , and q_I was developed to explain the observed fluorescence yields (Fig. 9). Photochemical quenching was described using the Kiefer and Reynolds (1992) model (Eqs. 1 and 2). Nonphotochemical quenching was modeled as an effective decrease in the probability of a photon reaching a reaction center capable of fluorescence, potentially achieved either through thermal dissipation of absorbed energy or photodamage of the reaction center. The decrease in ϕ_f with increasing irradiance was modeled using target theory, similar to that used for the number of open reaction centers, such that increasing irradiance decreased the number of available reaction centers. The complex dynamics of the slower part of nonphotochemical quenching, q_I , meant that no functional relationship with its controlling parameters was possible. For the discussion herein, q_I was varied systematically from 1 to 0 representing minimal and maximal quenching, respectively. To account for the apparently constant value of ϕ_f at high irradiances, it was assumed that there was a constant fraction of reaction centers, r , that were unaffected by nonphotochemical quenching. Nonphotochemical quenching was modeled using

$$q_N = r + (1 - r)q_I q_E = r + (1 - r)q_I e^{-E_0/E_T} \quad (17)$$

where E_T is the irradiance above which q_E approaches its maximum. Including this with the photochemical quenching model gave Eq. 18.

$$\phi_f = (r + [1 - r]q_I e^{-E_0/E_T})(\phi_{f_{\min}} A + \phi_{f_{\max}} [1 - A]) \quad (18)$$

The model may not describe the behavior of ϕ_f at irradiances below the inflection irradiance for profiles with high degrees of q_I because of the lack of ϕ_f measurements in this region. In the case that $\phi_{f_{\min}}$ is less affected by nonphotochemical quenching than $\phi_{f_{\max}}$ (Havaux et al. 1991), it may be appropriate to apply the q_N only to $\phi_{f_{\max}}$. A family of curves with varying levels of q_I was generated with the parameters selected to fit the observed data ($r = 0.04$, $E_k = 55 \mu\text{mol quanta m}^{-2} \text{ s}^{-1}$, $E_T = 350 \mu\text{mol quanta m}^{-2} \text{ s}^{-1}$, $\phi_{f_{\min}} = 0.030$, and $\phi_{f_{\max}} = 0.090$) and is shown in Fig. 9.

Inherent in this model is the assumption that the timescale of mixing for the surface mixed layer is less than that for relaxation of q_I , which results in a uniform distribution of q_I with depth for any given cast. The model also ascribes the quenching with increased irradiance described by target theory solely to q_E . In reality, q_I may vary with depth depending on the interaction of the mixing timescales and the onset and relaxation kinetics of q_I , and q_E alone may be insufficient to allow maximum quenching associated with high irradiances that may also include contributions from q_I (Horton et al. 1996). Interpretation of the observations and results of the model is complicated by the uncertainty associated with partitioning of q_N and the mechanisms associated with q_I , thermal energy dissipation, and/or PSII reaction center damage (Krause and Weis 1991; Horton et al. 1996). The effects of nutrient limitation are beyond the scope of the present work but could be hypothesized to affect q_I .

Despite the limitations of the model, some interesting conclusions about the photophysiology of phytoplankton can be made. The convergence of ϕ_f at irradiances of $2,000 \mu\text{mol quanta m}^{-2} \text{ s}^{-1}$ may be of evolutionary significance, because this corresponds to full sunlight, when photoprotection would be expected to be maximal. In the context of the model, the fraction of viable reaction centers that fluoresce at these irradiance, r , was 4%, which may reflect either the recovery rate of damaged reaction centers—for example, by replacement of damaged D1 proteins (Han et al. 2000; Zhang et al. 2000)—or the fraction of reaction centers that are not bypassed by thermal dissipation of the excitation energy. It should be noted that the interpretations of the model are limited by the assumptions made in its formulation and that there are other possible explanations for the asymptotic relationship of ϕ_f with irradiance.

Implications for interpretation of fluorescence-based measurements—Knowledge of the variation in ϕ_f is essential for the interpretation of fluorescence-based measurements. The large range in ϕ_f observed herein and in previous work refutes the paradigm of a constant ϕ_f necessary for accurate assessment of phytoplankton biomass using sun-stimulated fluorescence measurements. With greater ranges in biomass, the apparent error associated with variations in ϕ_f would be reduced. As such, sun-stimulated fluorescence is generally only a gross indicator of biomass (Roesler and Perry 1995). The dominance of nonphotochemical quenching in surface waters and the uncertainties in the relationship between the quantum yields of fluorescence and photochemistry with q_N suggest that sun-stimulated fluorescence may be a poor indicator of primary production. A greater understanding of the effect of nonphotochemical quenching on the quantum yields of fluorescence and photochemistry may improve this. It should be noted that the fluorescence output and primary production would be expected to covary, given that one of the major sources of variation in both is the absorbed excitation energy.

One interesting case is that of satellite-derived measurements of ocean color and the fluorescence signal. As noted by Maritorena et al. (2000), the near-noon equator-crossing time of polar orbiting satellites and the shallow depth of the signal results in measurements of sun-stimulated fluorescence only at high irradiances. Initial results presented here suggest that the range of ϕ_f under these conditions is small, which could result in improved estimation of biomass concentrations. Concurrent ϕ_f estimates could provide interesting information into the physiological state of the phytoplankton in this very shallow layer of the oceans. Further work is needed to investigate the temporal and spatial distribution of ϕ_f and its consistency at high irradiances. The methods presented herein provide the basis for achieving this not only from in-water but also from above-water measurements.

References

- AHN, Y. H., A. BRICAUD, AND A. MOREL. 1992. Light backscattering efficiency and related properties of some phytoplankters. *Deep-Sea Res.* **39**: 1835–1855.

- BABIN, M., A. MOREL, AND B. GENTILI. 1996. Remote sensing of sea surface sun-induced chlorophyll fluorescence: Consequences of natural variations in the optical characteristics of phytoplankton and the quantum yield of chlorophyll a fluorescence. *Int. J. Remote Sens.* **17**: 2417–2448.
- , J. THERIAULT, L. LEGENDRE, AND A. CONDAL. 1993. Variations in the specific absorption coefficient for natural phytoplankton assemblages: Impact on estimates of primary production. *Limnol. Oceanogr.* **38**: 154–177.
- BERWALD, J., D. STRAMSKI, C. D. MOBLEY, AND D. A. KIEFER. 1998. Effect of Raman scattering on the average cosine and diffuse attenuation coefficient of irradiance in the ocean. *Limnol. Oceanogr.* **43**: 564–576.
- BIDIGARE, R. R., R. C. SMITH, K. S. BAKER, AND J. MARRA. 1987. Oceanic primary production estimates from measurements of spectral irradiance and pigment concentrations. *Global Biogeochem. Cycles* **1**: 171–186.
- BIRD, R. E. 1984. A simple, solar spectral model for direct-normal and diffuse horizontal irradiance. *Sol. Energy* **32**: 461–471.
- BRICAUD, A., A. MOREL, AND L. PRIEUR. 1981. Absorption by dissolved organic matter of the sea (yellow substance) in the UV and visible domains. *Limnol. Oceanogr.* **26**: 45–53.
- CHAMBERLIN, W. S., C. R. BOOTH, D. A. KIEFER, J. H. MORROW, AND R. C. MURPHY. 1990. Evidence for a simple relationship between natural fluorescence, photosynthesis and chlorophyll in the sea. *Deep-Sea Res.* **37**: 951–973.
- , AND J. MARRA. 1992. Estimation of photosynthetic rate from measurements of natural fluorescence: Analysis of the effects of light and temperature. *Deep-Sea Res.* **39**: 1695–1706.
- CLEVELAND, J. S., AND A. D. WEIDEMANN. 1993. Quantifying absorption by aquatic particles: A multiple scattering correction for glass-fiber filters. *Limnol. Oceanogr.* **38**: 1321–1327.
- COLLINS, D. J., D. A. KIEFER, J. B. SOOHOO, AND I. S. MCDERMID. 1985. The role of reabsorption in the spectral distribution of phytoplankton fluorescence emission. *Deep-Sea Res.* **32**: 983–1003.
- CULVER, M. E., AND M. J. PERRY. 1997. Calculation of solar-induced fluorescence in surface and subsurface waters. *J. Geophys. Res.* **102**: 10563–10572.
- DANDONNEAU, Y., AND J. NEVEUX. 1997. Diel variations of in vivo fluorescence in the eastern equatorial Pacific: An unvarying pattern. *Deep-Sea Res. II* **44**: 1869–1880.
- DEMMIG-ADAMS, B. 1990. Carotenoids and photoprotection in plants: A role for the xanthophyll zeaxanthin. *Biochim. Biophys. Acta.* **1020**: 1–24.
- , AND W. W. I. ADAMS. 1992. Photoprotection and other responses of plants to high light stress. *Annu. Rev. Plant Physiol. Plant Mol. Biol.* **43**: 599–626.
- DOERFFER, R. 1981. Factor analysis in ocean color interpretation, p. 339–345. *In* J. F. R. Gower [ed.], *Oceanography from space*. Plenum.
- . 1993. Estimation of primary production by observation of solar-stimulated fluorescence, p. 104–113. *In* K. W. Li and S. Y. Maestrini [eds.], *Measurement of primary production from molecular to the global scale*. ICES Marine Science Symposium.
- ESAIAS, W. E., AND OTHERS. 1998. An overview of MODIS capabilities for ocean science observations. *IEEE Trans. Geosci. Remote Sens.* **36**: 1250–1265.
- FALKOWSKI, P., AND D. A. KIEFER. 1985. Chlorophyll *a* fluorescence in phytoplankton: Relationship to photosynthesis and biomass. *J. Plankton Res.* **7**: 715–731.
- FALKOWSKI, P. G., AND Z. KOLBER. 1995. Variations in the chlorophyll fluorescence yields in the phytoplankton in the world oceans. *Aust. J. Plant Physiol.* **22**: 341–355.
- , AND J. LAROCHE. 1991. Acclimation to spectral irradiance in algae. *J. Phycol.* **27**: 8–14.
- , AND J. A. RAVEN. 1997. *Aquatic photosynthesis*. Blackwell.
- FISCHER, J., AND U. KRONFELD. 1990. Sun-stimulated chlorophyll fluorescence—part 1: Influence of oceanic properties. *Int. J. Remote Sens.* **11**: 2125–2147.
- GARVER, S. A., AND D. A. SIEGEL. 1997. Inherent optical property inversion of ocean color spectra and its biogeochemical interpretation. 1. Time series from the Sargasso Sea. *J. Geophys. Res.* **102**: 18,607–18,625.
- GORDON, H. R. 1979. Diffuse reflectance of the ocean: The theory of its augmentation by chlorophyll a fluorescence at 685 nm. *Appl. Opt.* **18**: 1161–1166.
- , O. R. BROWN, R. E. EVANS, J. W. BROWN, R. C. SMITH, K. S. BAKER, AND D. C. CLARK. 1988. A semianalytic model of ocean color. *J. Geophys. Res.* **93**: 10,909–10,924.
- GOWER, J. F. R. 1980. Observations of fluorescence of in situ chlorophyll-*a* in Saanich Inlet. *Boundary-Layer Meteorol.* **18**: 235–245.
- , R. DOERFFER, AND G. A. BORSTAD. 1999. Interpretation of the 685 nm peak in water-leaving radiance spectra in terms of fluorescence, absorption and scattering, and its observation by MERIS. *Int. J. Remote Sens.* **20**: 1771–1786.
- HALTRIN, V. I., AND G. KATTAWAR. 1991. Light fields with Raman scattering and fluorescence in sea water. Dept. of Physics, Texas A&M Univ.
- HAN, B.-P., M. VIRTANEN, J. KOPONEN, AND M. STRASKRABA. 2000. Effect of photoinhibition on algal photosynthesis: A dynamic model. *J. Plankton Res.* **22**: 865–885.
- HAVAUX, M., R. STASSER, AND H. GREPPING. 1991. A theoretical and experimental analysis of the qp and qn coefficients of chlorophyll fluorescence and their relation to photochemical and nonphotochemical events. *Photosynth. Res.* **27**: 41–55.
- HOEPPFNER, N., AND S. SATHYENDRANATH. 1993. Determination of the major groups of phytoplankton pigments from the absorption spectra of total particulate matter. *J. Geophys. Res.* **98**: 22,789–22,803.
- HORTON, P., A. V. RUBAN, AND R. G. WALTERS. 1996. Regulation of light harvesting in green plants. *Annu. Rev. Plant Physiol. Plant Mol. Biol.* **47**: 655–684.
- HU, C., AND K. J. VOSS. 1998. Measurement of solar-stimulated fluorescence in natural waters. *Limnol. Oceanogr.* **43**: 1198–1206.
- KIEFER, D. 1973. Fluorescence properties of natural phytoplankton populations. *Mar. Biol.* **22**: 263–269.
- , W. S. CHAMBERLIN, AND C. R. BOOTH. 1989. Natural fluorescence of chlorophyll *a*: Relationship to photosynthesis and chlorophyll concentration in the western South Pacific gyre. *Limnol. Oceanogr.* **34**: 868–881.
- , AND R. A. REYNOLDS. 1992. Advances in understanding phytoplankton fluorescence and photosynthesis, p. 155–174. *In* P. G. Falkowski and A. D. Woodhead [eds.], *Primary productivity and biogeochemical cycles in the sea*. Plenum.
- KINKADE, C. S., J. MARRA, T. D. DICKEY, C. LANGDON, D. E. SIGURDSON, AND R. WELLER. 1999. Diel bio-optical variability observed from moored sensors in the Arabian Sea. *Deep-Sea Res. II* **46**: 1813–1831.
- KIRK, J. T. O. 1991. Volume scattering function, average cosines, and the underwater light field. *Limnol. Oceanogr.* **36**: 455–467.
- KISHINO, M., S. SUGIHARA, AND N. OKAMI. 1984. Influence of fluorescence of chlorophyll a on the underwater upward irradiance spectrum. *Mer* **22**: 224–232.
- KRAUSE, G. H., AND E. WEIS. 1991. Chlorophyll fluorescence and photosynthesis: The basics. *Annu. Rev. Plant Physiol.* **42**: 313–349.

- LI, X.-P., O. BJOERKMAN, C. SHIH, A. R. GROSSMAN, M. ROSENQUIST, S. JANSSON, AND K. K. NIYOGI. 2000. A pigment-binding protein essential for regulation of photosynthetic light harvesting. *Nature* **403**: 391–395.
- LOHRENZ, S. E. 2000. A novel theoretical approach to correct for pathlength amplification and variable sampling loading in measurements of particulate spectral absorption by the quantitative filter technique. *J. Plankton Res.* **22**: 639–657.
- MARITORENA, S., A. MOREL, AND B. GENTILI. 2000. Determination of the fluorescence quantum yield by oceanic phytoplankton in their natural habitat. *Appl. Opt.* **39**: 6725–6737.
- MARRA, J. 1997. Analysis of diel variability in chlorophyll fluorescence. *J. Mar. Res.* **55**: 767–784.
- MARSHALL, B. R., AND R. C. SMITH. 1990. Raman scattering and in-water ocean optical properties. *Appl. Opt.* **29**: 71–84.
- MITCHELL, B. G. 1990. Algorithms for determining the absorption coefficient of aquatic particulates using the quantitative filter technique (QFT). *SPIE* **1302**: 137–148.
- MOBLEY, C. D. 1994. Light and water: Radiative transfer in natural waters. Academic.
- MOREL, A. 1974. Optical properties of pure water and seawater, p. 1–24. *In* N. G. Jerlov and E. S. Nielsen [eds.], *Optical aspects of oceanography*. Academic.
- , AND A. BRICAUD. 1981. Theoretical results concerning light absorption in a discrete medium, and application to specific absorption of phytoplankton. *Deep-Sea Res.* **28**: 1375–1393.
- MYERS, J., AND J. R. GRAHAM. 1963. Enhancement in *Chlorella*. *Plant Physiol.* **28**: 105–116.
- NEALE, P. J., AND P. J. RICHERSON. 1987. Photoinhibition and the diurnal variation of phytoplankton photosynthesis. I. Development of a photosynthesis-irradiance model from studies of in situ responses. *J. Plankton Res.* **9**: 167–193.
- NEVILLE, R. A., AND J. F. R. GOWER. 1977. Passive remote sensing of phytoplankton via chlorophyll *a* fluorescence. *J. Geol. Res.* **82**: 3487–3493.
- O'REILLY, J. E., AND OTHERS. 1998. Ocean color chlorophyll algorithms for SeaWiFS. *J. Geophys. Res.* **103**: 24,937–24,953.
- PETZOLD, T. J. 1972. Volume scattering functions for selected ocean waters. *Scripts Inst. Oceanogr., Visibility Lab., San Diego, CA*. SIO Ref. 72–78, 79 p.
- POPE, R. M., AND E. S. FRY. 1997. Absorption spectrum (300–700 nm) of pure water. II. Intergrating cavity measurements. *Appl. Opt.* **36**: 8710–8723.
- PRÉZELIN, B. B., AND A. C. LEY. 1980. Photosynthesis and chlorophyll *a* fluorescence rhythms of marine phytoplankton. *Mar. Biol.* **55**: 295–307.
- ROESLER, C. S. 1998. Theoretical and experimental approaches to improve the accuracy of particulate absorption coefficients derived from the quantitative filter technique. *Limnol. Oceanogr.* **43**: 1649–1660.
- , AND M. J. PERRY. 1995. In situ phytoplankton absorption, fluorescence emission, and particulate backscattering spectra determined from reflectance. *J. Geophys. Res.* **100**: 13,279–13,294.
- SIEGEL, D. A., A. F. MICHAELS, J. C. SORENSEN, M. C. O'BRIEN, AND M. A. HAMMER. 1995. Seasonal variability of light availability and utilization in the Sargasso Sea. *J. Geophys. Res.* **100**: 8695–8713.
- SOSIK, H. M., S. W. CHISHOLM, AND R. J. OLSON. 1989. Chlorophyll fluorescence from single cells: Interpretation of flow cytometric signals. *Limnol. Oceanogr.* **34**: 1749–1761.
- STEGMANN, P. M., M. R. LEWIS, C. O. DAVIS, AND J. J. CULLEN. 1992. Primary production estimates from recordings of solar-stimulated fluorescence in the equatorial Pacific at 150 W. *J. Geophys. Res.* **97**: 627–638.
- TASSAN, S., AND G. M. FERRARI. 1995. An alternative approach to absorption measurements of aquatic particles retained on filters. *Limnol. Oceanogr.* **40**: 1358–1368.
- , ———, A. BRICAUD, AND M. BABIN. 2000. Variability of the amplification factor of light absorption by filter-retained aquatic particles in the coastal environment. *J. Plankton Res.* **22**: 659–668.
- TETT, P. B. 1987. Plankton, p. 280–341. *In* J. M. Baker and W. J. Wolff [eds.], *Biological surveys of estuaries and coasts*. Cambridge Univ. Press.
- TOPLISS, B. J. 1985. Optical measurements in the Sargasso sea: Solar stimulated chlorophyll fluorescence. *Oceanol. Acta* **8**: 263–270.
- , AND T. PLATT. 1986. Passive fluorescence and photosynthesis in the ocean: implications for remote sensing. *Deep-Sea Res.* **33**: 849–864.
- WALRAFEN, G. E. 1967. Raman spectral studies of the effects of temperature on water structure. *J. Chem. Phys.* **47**: 114–126.
- . 1969. Continuum model of water—an erroneous interpretation. *J. Chem. Phys.* **50**: 567–569.
- YENTSCH, C. S. 1962. Measurement of visible light absorption by particulate matter in the ocean. *Limnol. Oceanogr.* **7**: 207–217.
- ZHANG, L., V. PAAKKARINEN, K. J. VAN WIJK, AND E. M. ARO. 2000. Biogenesis of the chloroplast-encoded d1 protein: regulation of translation elongation, insertion, and assembly into photosystem II. *Plant Cell* **12**: 1769–1782.

Received: 31 January 2002

Accepted: 21 October 2002

Amended: 14 November 2002